

# A small survey of the magnetic fields of planet-host stars\*

R. Fares<sup>1</sup>†, C. Moutou<sup>2</sup>, J.-F. Donati<sup>3</sup>, C. Catala<sup>4</sup>, E. Shkolnik<sup>5</sup>, M.M. Jardine<sup>1</sup>  
A.C. Cameron<sup>1</sup>, M. Deleuil<sup>2</sup>

<sup>1</sup> School of Physics and Astronomy, Univ. of St Andrews, St Andrews, Scotland KY16 9SS, UK

<sup>2</sup> Aix Marseille Université, CNRS, LAM, UMR 7326, F-13388, Marseille, France

<sup>3</sup> IRAP-UMR 5277, CNRS & Univ. de Toulouse, 14 Av. E. Belin F-31400 Toulouse, France

<sup>4</sup> Observatoire de Paris, 61 avenue de l'Observatoire F-75014 Paris, France

<sup>5</sup> Lowell Observatory, 1400 West Mars Hill Road, Flagstaff, AZ 86001, USA

2013, MNRAS, submitted

## ABSTRACT

Using spectropolarimetry, we investigate the large-scale magnetic topologies of stars hosting close-in exoplanets. A small survey of ten stars has been done with the twin instruments TBL/NARVAL and CFHT/ESPaDOnS between 2006 and 2011. Each target consists of circular-polarization observations covering 7 to 22 days. For each of the 7 targets in which a magnetic field was detected, we reconstructed the magnetic field topology using Zeeman-Doppler imaging. Otherwise, a detection limit has been estimated. Three new epochs of observations of  $\tau$  Boo are presented, which confirm magnetic polarity reversal. We estimate that the cycle period is 2 years, but recall that a shorter period of 240 days can not still be ruled out. The result of our survey is compared to the global picture of stellar magnetic field properties in the mass-rotation diagram. The comparison shows that these giant planet-host stars tend to have similar magnetic field topologies to stars without detected hot-Jupiters. This needs to be confirmed with a larger sample of stars.

**Key words:** stars: magnetic fields – stars: planetary systems – stars: activity – stars: individual – techniques: spectropolarimetry

## 1 INTRODUCTION

The role of the stellar magnetic field in the evolution of stellar and planetary systems is suspected to be important, but poorly constrained by observations. For instance, stellar magnetic braking, planet migration, and dynamical evolution may be acting simultaneously in the early stages of evolution of the systems, with an impact on the final state that depends on the system properties (Dobbs-Dixon et al. 2004; Lai et al. 2011). In the case of short-period planets, the interactions between the planet and the star continue throughout the lifetime of the system, as the planet may be embedded in the magnetosphere of the star at only a few stellar radii from the star's surface. The impact of the stellar wind may then be important (Vidotto et al. 2012), and even reconnections between the stellar and planetary magnetic fields could happen (Cohen et al. 2010, 2011; Lanza 2012). This can influence the planetary magnetic

field, the planetary upper atmosphere and maybe the internal structure of the planet as well. On the stellar side, the close-in planet, especially when it is massive, may induce anomalies on the stellar surface through magnetic interactions (Shkolnik et al. 2003, 2005; Walker et al. 2008; Pagano et al. 2009), although several observational searches for such signatures give results that are either unconfirmed, intermittent or difficult to interpret (e.g., Cranmer & Saar (2007); Shkolnik et al. (2008); Fares et al. (2012)). In order to better understand the environment where a close-in planet orbits its star, it is necessary to have information about the stellar magnetic field topology. Then, extrapolation techniques may be used to get quantified properties of the magnetic environment that may impact the planet (Jardine et al. 2002; Fares et al. 2010, 2012).

In this paper, we investigate the large-scale magnetic properties of ten planet-host stars using spectropolarimetric observations, in order to provide inputs to 1) more intensive similar campaigns on stars where the magnetic field is strong enough for an accurate characterization, and 2) extrapolation models that explore the star-planet magnetic

\* Based on observations obtained by NARVAL at Télescope Bernard Lyot (CNRS) and ESPaDOnS at Canada-France-Hawaii telescope.

† E-mail: rf60@st-andrews.ac.uk

interactions. Three new epochs of observations are reported for the short-cycle  $\tau$  Boo star, which makes 8 the total number of epochs when we observed this star. In Section 2, we describe the observational method and material, in Section 3 we present the stellar sample, and in Section 4 we discuss the results before concluding.

## 2 OBSERVATIONS

We have secured spectropolarimetric observations of stars hosting close-in extrasolar planets, using either ESPaDOnS at the 3.6-m Canada-France-Hawaii Telescope on Mauna Kea or NARVAL at the 2-m Telescope Bernard Lyot in Pic du Midi (France). Both instruments are twin high-resolution spectropolarimeters that measure the circular polarisation in stellar spectral lines using multiple exposures. The spectral resolution and range are respectively 65000 and 370-1000 nm in the polarisation mode. Four exposures per observation are necessary to derive the circular polarisation (Stokes V) profiles and check its significance with respect to spurious polarisation signals. The data were collected between June 2006 and January 2011, over a sample of 10 planet-host stars. For some stars of our sample, the number of collected spectra is limited, as they correspond to a first-investigation survey for spectropolarimetric detections in preparation for more intensive follow-up observations of detected fields. Table 1 gives a summary of the observations performed in this program.

The data were reduced with the software LIBRE-ESPRIT that automatically extracts and calibrates intensity and polarization spectra. The Least-Square-Deconvolution (LSD, Donati et al. 1997) profiles are calculated to significantly improve the SNR, using a mask adapted to the spectral type of each target. On average, more than 6000 stellar lines are used to produce these intensity and polarisation profiles. The LSD profiles are corrected for the radial-velocity shift of the star, including the motion due to the planet. The radial-velocity precision of the stellar intensity profiles are better than  $30 \text{ m s}^{-1}$ .

## 3 STELLAR PROPERTIES

The stellar sample selected for our study includes 10 stars brighter than  $V = 12$ , hosting planets at orbital periods less than 11 days. Most of these planets are giant planets with masses larger than  $0.22 M_{Jup}$ , except CoRoT-7 b which is a telluric planet in an extremely short orbit ( $0.015 M_{Jup}$  and 0.85 day period, Léger et al. 2009). The stellar parameters adopted in this work are summarized in Table 2. The rotation periods are a critical parameter, and often the least constrained one. The targets were originally selected for their short rotational periods, in order to allow observations with the two-week runs with ESPaDOnS; this does not apply, however, for HD 46375 and CoRoT-7, which were selected because of existing data of the CoRoT satellite (despite their long rotational periods). Note also that the rotation period of HD 130322 was recently updated to 26 days (Simpson et al. 2010) while it was given as 12 days in the planet discovery paper (Udry et al. 2000). There is

also contradiction in the literature about the rotation period of HD 102195 (12 days in Ge et al. (2006) and 20 days in Melo et al. (2007)): in our analysis, we choose the 12-day value which is based on photometric observations rather than on activity calibrations.

Concerning the stellar inclination, we use in general the value derived from the chosen rotation period, with  $\sin i = v \sin i \times P_{rot} / (2\pi R_*)$ . The reconstruction of the stellar magnetic field is, however not very sensitive to a precise knowledge of the inclination (up to  $20^\circ$ , Morin et al. 2008).

## 4 SPECTROPOLARIMETRIC ANALYSES

When a sufficient number of detected Stokes V profiles is available, we reconstruct the best-fit magnetic topology using a tomographic technique called Zeeman Doppler Imaging (ZDI) as developed by Donati et al. (1997, 2006) and described in these papers. ZDI consists of inverting series of Stokes V profiles into the stellar magnetic field topology responsible for producing these profiles. The problem is ill-posed, ZDI uses the principles of maximum entropy to retrieve the simplest image compatible with the data. The magnetic field is described by its radial, azimuthal and meridional components, all expressed in terms of spherical harmonics expansions. This description of the field allows to calculate easily the contribution of each spherical harmonic order to the field, as well as the contribution of the poloidal and toroidal components and the degree of axisymmetry. Note that the axisymmetric contribution is given by modes with  $m < l/2$ .

### 4.1 The evolution of magnetic topology $\tau$ Boo

Previous spectropolarimetric analyses of 5 epochs of observations of  $\tau$  Boo (F7V) have been described in Catala et al. (2007), Donati et al. (2008) and Fares et al. (2009). These data showed two occurrences of polarity reversals. The derived length of the magnetic cycle was about two years; the temporal sampling of the observations, however, allowed other possible values for the cycle period.

New data were acquired with TBL/NARVAL during three separate epochs, in May 2009 (data spanning 19 days), January 2010 (20 days) and January 2011 (12 days). The journal of these new observations is shown in appendix A (Table A1).

The LSD profiles were calculated using the same method and parameters as in Fares et al. (2009). We reconstructed the magnetic topology of  $\tau$  Boo for all three epochs using the differential rotation (hereafter DR) measured by Fares et al. (2009). We used up to 8 degrees of spherical harmonics and an inclination of  $45^\circ$ . Our measurements of the inclination using ZDI in Catala et al. (2007), Donati et al. (2008) and Fares et al. (2009) agrees with the measurements of Rodler et al. (2013) and Brogi et al. (2012) who used a different technique. We fit the V profiles to a level of reduced chi-square  $\chi_r^2 = 0.95$ . The observed and fitted profiles are shown in Figure 1. The maps projected on a spherical coordinate system are shown in Figure 2.

Previous observations have shown a large DR in  $\tau$  Boo, with a surface shear of the order of  $d\Omega = 0.4 \pm 0.1 \text{ rad d}^{-1}$  and an equatorial angular velocity of  $\Omega_{eq} = 2.0 \pm 0.1 \text{ rad d}^{-1}$

**Table 1.** Summary of observations and results presented in this paper. The instrument used is either CFHT/ESPaDOnS (ESP) or TBL/NARVAL (NAR). The epochs of observations and numbers of spectra (# seq) are listed. Detection status is N: no detection, Y: few detections, M: several detections and map reconstruction. The mean magnetic field strength (B), the percentage of poloidal energy over total magnetic energy (Pol) and the percentage of axisymmetry in the poloidal field are given for all epochs. When there is no detection, an upper limit is given for B for an adopted peculiar magnetic topology (and thus poloidal contribution).

Name	Instrument	Date	# seq	Detection	B (G)	% Pol	% Axisy	Ref
HD 46375	ESP	Jan08	10	Y-M	2	99	78	this work
HD 46375	NAR	Sep08	18	M	3.2			Gaulme et al. (2010)
HD 73256	ESP	Jan08	9	M	2.7	80	4	this work
HD 102195	ESP	Jan08	10	M	12.4	44	25	this work
HD 130322	ESP	Jan08	9	M	2.5	84	58	this work
HAT-P-2	ESP	Jan08	4	N	<40	75	-	this work
HD 179949	ESP	Jun07	19	M	2.6	80	55	Fares et al. (2012)
HD 179949	ESP	Sep09	10	M	3.7	90	36	Fares et al. (2012)
HD 189733	ESP	Jun06	19	M	33	77	56	Moutou et al. (2007)
HD 189733	NAR	Jun07	20	M	22	43	26	Fares et al. (2010)
HD 189733	NAR	Jul08	24	M	36	33	17	Fares et al. (2010)
CoRoT-7	NAR	Jan10	4	N	<150	100	-	this work
$\tau$ Bootis	ESP	Jun06	12	M	1.8			Catala et al. (2007)
$\tau$ Bootis	NAR/ESP	Jun07	2/30	M	3.7	83	60	Donati et al. (2008)
$\tau$ Bootis	ESP	Jan08	40	M	3.1	38	20	Fares et al. (2009)
$\tau$ Bootis	NAR	Jun08	9	M	2.3	87	36	Fares et al. (2009)
$\tau$ Bootis	NAR	Jul08	19	M	1.7	91	62	Fares et al. (2009)
$\tau$ Bootis	NAR	Jun09		M	2.7	88	43	this work
$\tau$ Bootis	NAR	Jan10		M	3.8	62	46	this work
$\tau$ Bootis	NAR	Jan11		M	3.2	70	37	this work
XO-3	ESP	Jan08	15	N	<20	90	-	this work

**Table 2.** Fundamental parameters of stars used in this work and some properties of their planets. The columns list the name of the star, its visual magnitude, spectral type, effective temperature, log of the gravity at the surface, [Fe/H], stellar mass, stellar radius,  $v \sin i$ , rotation period, orbital period of the planet, semi-major axis of the planetary orbit, planet's projected mass and the references.

Name	Vmag	SpT	$T_{\text{eff}}$ K	$\log g$	[Fe/H]	$M_{\star}$ $M_{\odot}$	$R_{\star}$ $R_{\odot}$	$v \sin i$ km s $^{-1}$	$P_{\text{rot}}$ days	$P_{\text{orb}}$ days	$a$ AU	$M_p \sin i$ $M_{Jup}$	Ref. <sup>1</sup>
HD 46375	7.9	K1IV	5290	4.66	0.39	0.97	0.86	1.2	42	3.0236	0.0399	0.2272	G10,B06
HD 73256	8.08	G8	5636	4.30	0.26	1.05	0.89	3.2	14	2.5486	0.0371	1.869	B06,U03
HD 102195	8.05	K0V	5290	4.45	0.05	0.87	0.82	2.9	12.3	4.1138	0.0479	0.453	G06,M07
HD 130322	8.04	K0V	5330	4.41	-0.02	0.79	0.83	1.6	26.1	10.708	0.0896	1.043	U00,S10
HAT-P-2	8.71	F8	6290	4.22	0.12	1.36	1.64	20.8	3.8	5.6335	0.0687	9.09	P10
HD 179949	6.25	F8V	6168	4.34	0.14	1.21	1.19	7.0	7.6	3.0925	0.0439	0.902	B06,F12
HD 189733	7.7	K2V	5050	4.59	-0.03	0.82	0.76	2.97	12.5	2.2186	0.0310	1.140	B05,F10
CoRoT-7	11.7	G9V	5250	4.47	0.12	0.91	0.82	1.1	23.6	0.8536	0.0172	0.0151	B10
$\tau$ Bootis	4.5	F7V	6387	4.25	0.23	1.34	1.42	15.0	3.0	3.3124	0.0480	4.170	F09,B12
XO-3	9.8	F5V	6430	3.95	-0.18	1.41	2.08	18.3	3.7	3.1915	0.0454	11.79	JK08,W09

<sup>1</sup>G10: Gaulme et al. (2010),B06: Butler et al. (2006),U03: Udry et al. (2003),G06: Ge et al. (2006),M07: Melo et al. (2007), U00: Udry et al. (2000),S10: Simpson et al. (2010),P10: Pál et al. (2010),F12: Fares et al. (2012),B05: Bouchy et al. (2005),F10: Fares et al. (2010),B10: Bruntt et al. (2010),F09: Fares et al. (2009),B12: Brogi et al. (2012),JK08: Johns-Krull et al. (2008),W09: Winn et al. (2009)

(Donati et al. 2008; Fares et al. 2009). DR is again detected in the May 2009 data set, with corresponding values of  $\Omega_{\text{eq}} = 1.98 \pm 0.01 \text{ rad d}^{-1}$  and  $d\Omega = 0.15 \pm 0.03 \text{ rad d}^{-1}$ . The value of  $d\Omega$  is significantly smaller than values measured in previous epochs. Although our observations cover 20 days, the rotational phases do not sample the stellar surface very widely, which may induce a bias in deriving the DR. For this

reason, we reconstructed the maps using the DR parameters as measured in previous epochs, for all data.

The properties of the reconstructed magnetic maps for the three new epochs are summarized in Table 3. The average magnetic field ranges from 2.7 to 3.8 G, with values very similar to the ones reported in earlier analyses (1.7 to 3.7 G in Fares et al. 2009). The contribution of the toroidal

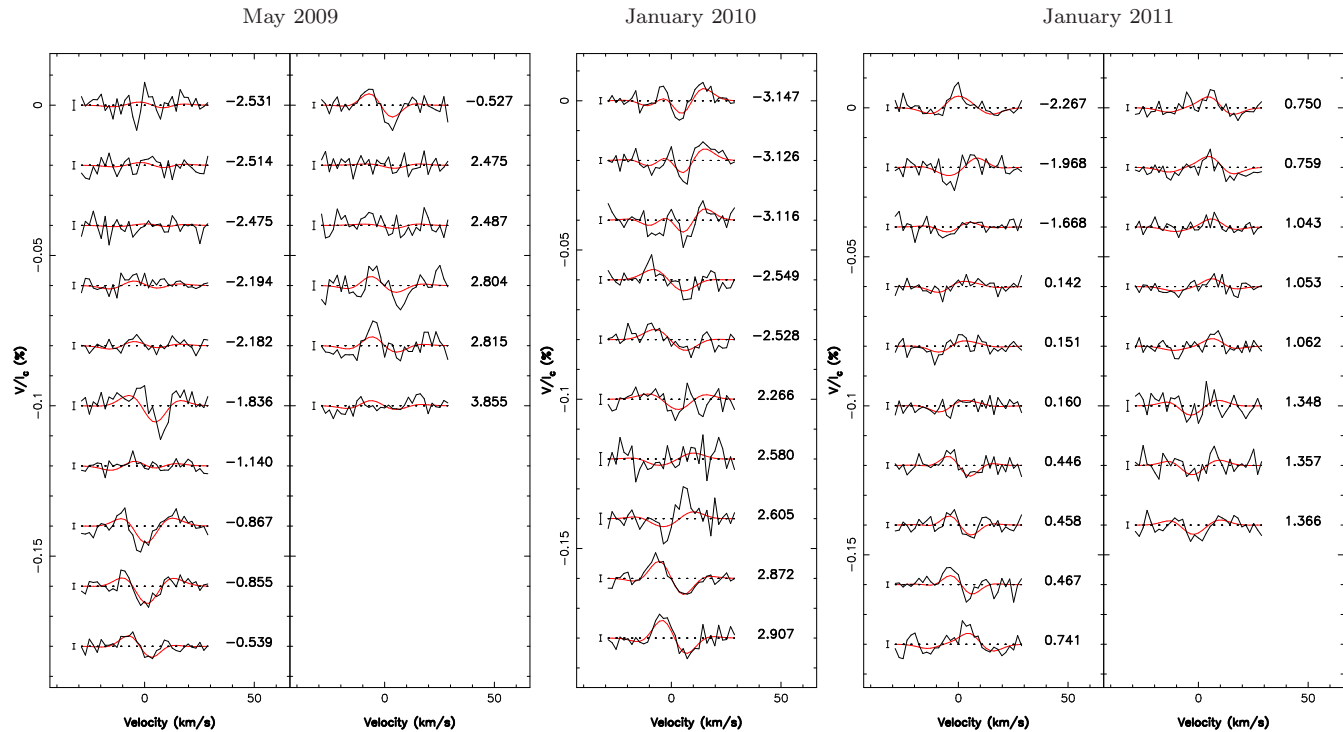


**Figure 1.** Circular polarization profiles of  $\tau$  Boo obtained in May 2009, January 2010 and January 2011 with TBL/NARVAL. The observed and synthetic profiles are shown in black and red, respectively. On the left of each profile we show a  $\pm 1\sigma$  error bar, while on the right the rotational cycles are indicated.

component to the total magnetic energy varies from 12 to 30%, in a smaller extent with respect to earlier epochs (9 to 62%). The last epoch of observation, in January 2011, shows a new polarity reversal compared to January 2010. In addition, the field has also switched polarity between July 2008 (last map in Fares et al. 2009) and May 2009. As observed earlier, the field configuration evolves inside a cycle: between May 2009 and January 2010, the energy distributed in the radial field has decreased while the energy in the azimuthal field has increased.

### Period of magnetic cycle

In order to determine the length of  $\tau$  Boo’s magnetic cycle, we performed a period search similar to the one described in Fares et al. (2009). We calculated the (signed) magnetic flux in both the radial and azimuthal component of the field for each reconstructed map. In the case of the radial field, the flux is counted positive for latitudes greater than  $30^\circ$ , and negative for latitudes between  $0^\circ$  and  $30^\circ$ . We then simultaneously fitted the two fluxes with two sine waves of equal period, the period being varied on a range of 100-1300 days. We found, as in Fares et al. (2009), two periods that fit the data well. The first one is of 740 days (2 years), and the second one is of 240 days (8 months), see Figure 3. We then calculated the false-alarm probability (FAP) of these periods. We produced 10000 data sets by night shuffling, and fitted each data set following the same procedure described above. The FAP is the number of data sets for which the  $\chi_r^2$  is smaller than the  $\chi_r^2$  of our periods divided by 10000.

We find a FAP of 3% for the 240 day period, and a FAP of 15% for the 740 day period.

### 4.2 HD 73256

Nine ESPaDOnS spectra of HD 73256 (G8) spanning 11 days were obtained in January 2008. Six circular polarisation signatures are detected. The adopted stellar inclination is  $75^\circ$  deduced from the rotational period measured by photometry (Udry et al. 2003). DR is not detected in the data and thus is fixed to zero for the reconstruction of the magnetic field. When correcting each LSD profile for the radial velocity of the star, we found that our measurements did not match the orbital ephemeris published in the literature,  $T_0=2452500.18 \pm 0.28$  (Udry et al. 2003). We updated the orbit phase using a measured  $T_0=2452500.42$ . The magnetic map is reconstructed for a  $\chi_r^2$  of 1.15, which produces a reasonable fit to the Stokes V profiles (Figure 4 first column). The magnetic field that best matches the observations is an 80% poloidal field with mean strength of 2.7 G. A small fraction of the the poloidal field is in axisymmetric modes ( $\sim 4\%$ ). The reconstructed topology of the stellar surface field is shown on Figure 5 (top row).

### 4.3 HD 102195

Ten spectra of HD 102195 (K0V) were obtained with ESPaDOnS in January 2008 (spanning 11 days), among which eight show a definite detection of the magnetic field. The data do not show any evidence for DR, we consider a solid rotation at the 12 day period measured by Ge et al. (2006)

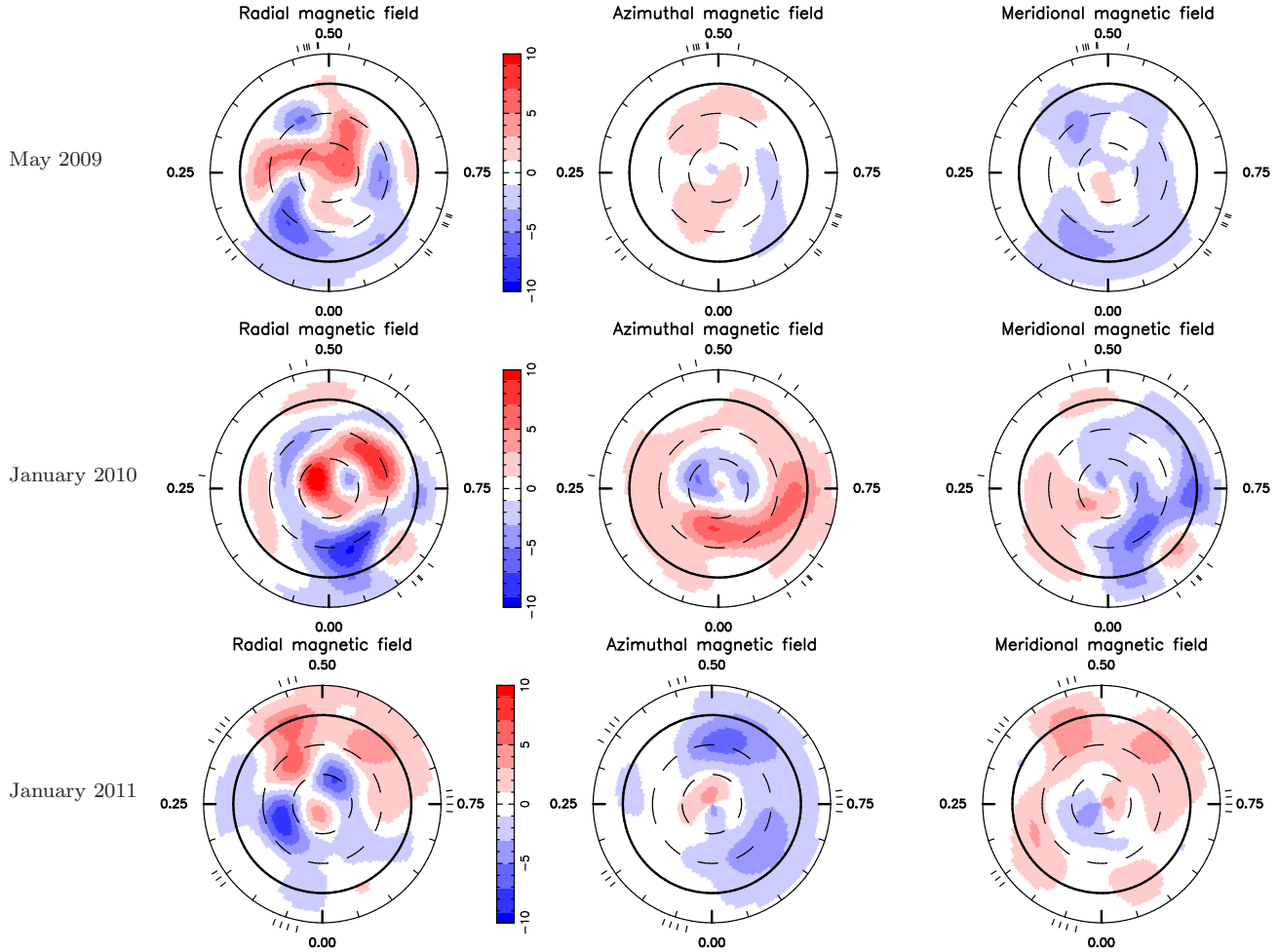


**Figure 2.** Magnetic topology of  $\tau$  Boo reconstructed from profiles in Figure 1: May 2009 (top row); January 2010 (middle row); January 2011 (bottom row). The radial, azimuthal and meridional components of the field (with magnetic field strength labelled in G) are depicted. The star is shown in flattened polar projection down to latitudes of  $30^\circ$ , with the equator depicted as a bold circle and parallels as dashed circles. Radial ticks around each plot indicate rotational phases of observations.

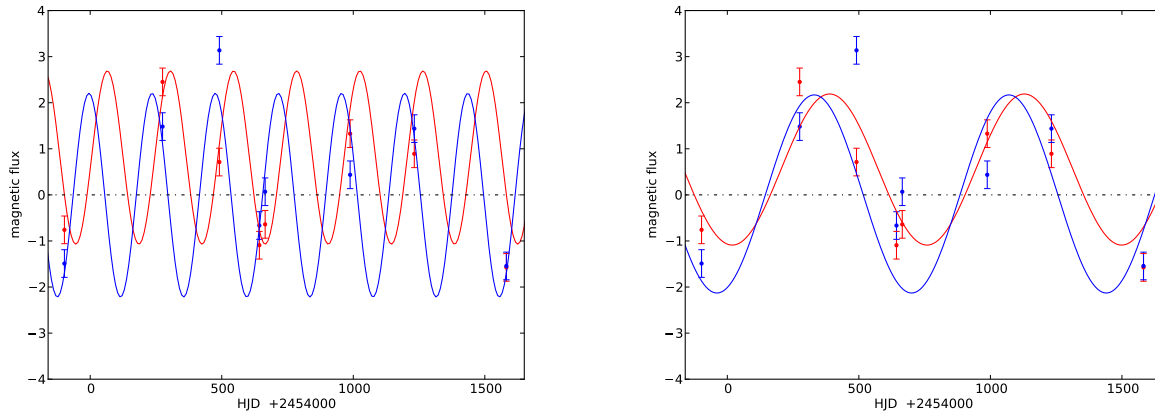


**Figure 3.** Fluxes of the radial field (red) and azimuthal field (blue) vs HJD, calculated for the Northern hemisphere of  $\tau$  Boo. In the particular case of  $B_r$ , the magnetic flux is counted positive for latitudes superior to  $30^\circ$  and negative for latitudes between  $0^\circ$  and  $30^\circ$  to take into account the contribution of both dipolar and quadrupolar terms of the poloidal field (as in Fares et al. 2009). The best sinusoidal fit for  $P = 240$  d (left panel) and  $P = 740$  d (right panel) are plotted.

**Table 3.** Summary of magnetic topology evolution of  $\tau$  Boo: average magnetic field B, percentage of the toroidal energy relative to the total energy, percentage of the energy contained in the axisymmetric modes of the poloidal component (modes with  $m < l/2$ ) and percentage of the energy contained in the modes of  $l \leq 2$  of the poloidal component for each epoch of observations.

Epoch	B (G)	% toroidal %	% axisym in poloidal %	% $l \leq 2$ in poloidal %	Reference
June 2007	3.7	17	60	52	Donati et al. (2008)
January 2008	3.1	62	20	50	Fares et al. (2009)
June 2008	2.3	13	36	36	Fares et al. (2009)
July 2008	1.7	9	62	47	Fares et al. (2009)
May 2009	2.7	12	43	47	this work
January 2010	3.8	38	46	40	this work
January 2011	3.2	30	37	50	this work

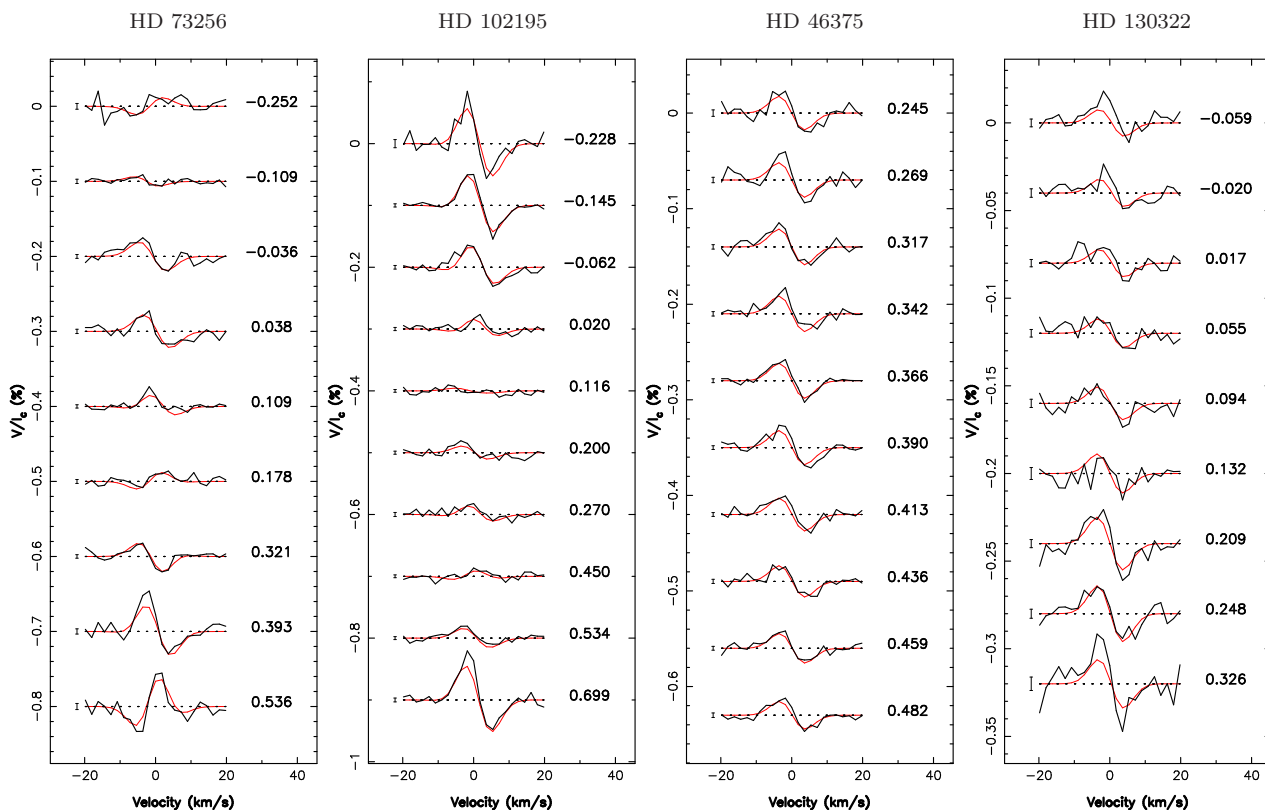


**Figure 4.** Circular polarization profiles obtained in January 2008 with CFHT/ESPADOnS for stars HD 73256, HD 102195, HD 46375 and HD 130322 respectively from left to right. See legend details in Figure 1.

and an inclination of  $50^\circ$  for the magnetic field reconstruction. The radial velocity of the star is corrected from the systemic velocity and the planet induced motion, as given in the literature (Melo et al. 2007). Our ESPADOnS observations are not of sufficient velocity precision to permit the detection of the planet signal, especially on this star that exhibits activity jitter (Melo et al. 2007).

Our observations cover almost one stellar rotation. The circular polarisation profiles are well fitted as shown in Figure 4 (second column). The field modelling is achieved for a  $\chi_r^2 = 1.2$ . The characteristics of the best-fit magnetic model features a dipole contributing by 70% to the poloidal component. The field's mean strength is of 12.5 G, 45% of the magnetic energy in the poloidal field (Figure 5, second row), and 25% of the poloidal field is axisymmetric.

#### 4.4 HD 46375

HD 46375 (K1IV) has been first observed with ESPADOnS in January 2008, and then with NARVAL in October 2008. This later data set has been obtained simultaneously with CoRoT photometric observations and is described in Gaulme et al. (2010). We describe in the following the data obtained with ESPADOnS, although its temporal coverage is much poorer: only one quarter of the rotational period has been covered. Such a poor sampling of the stellar surface prevents the reconstruction of a magnetic map. We just recall the properties of the field as characterized by the NARVAL observations in October 2008: the field is dominated by a slightly tilted and mostly axisymmetric dipole with respect to the rotation axis; the magnetic strength at the pole is of the order of 5 G. The Stokes V profiles observed in January

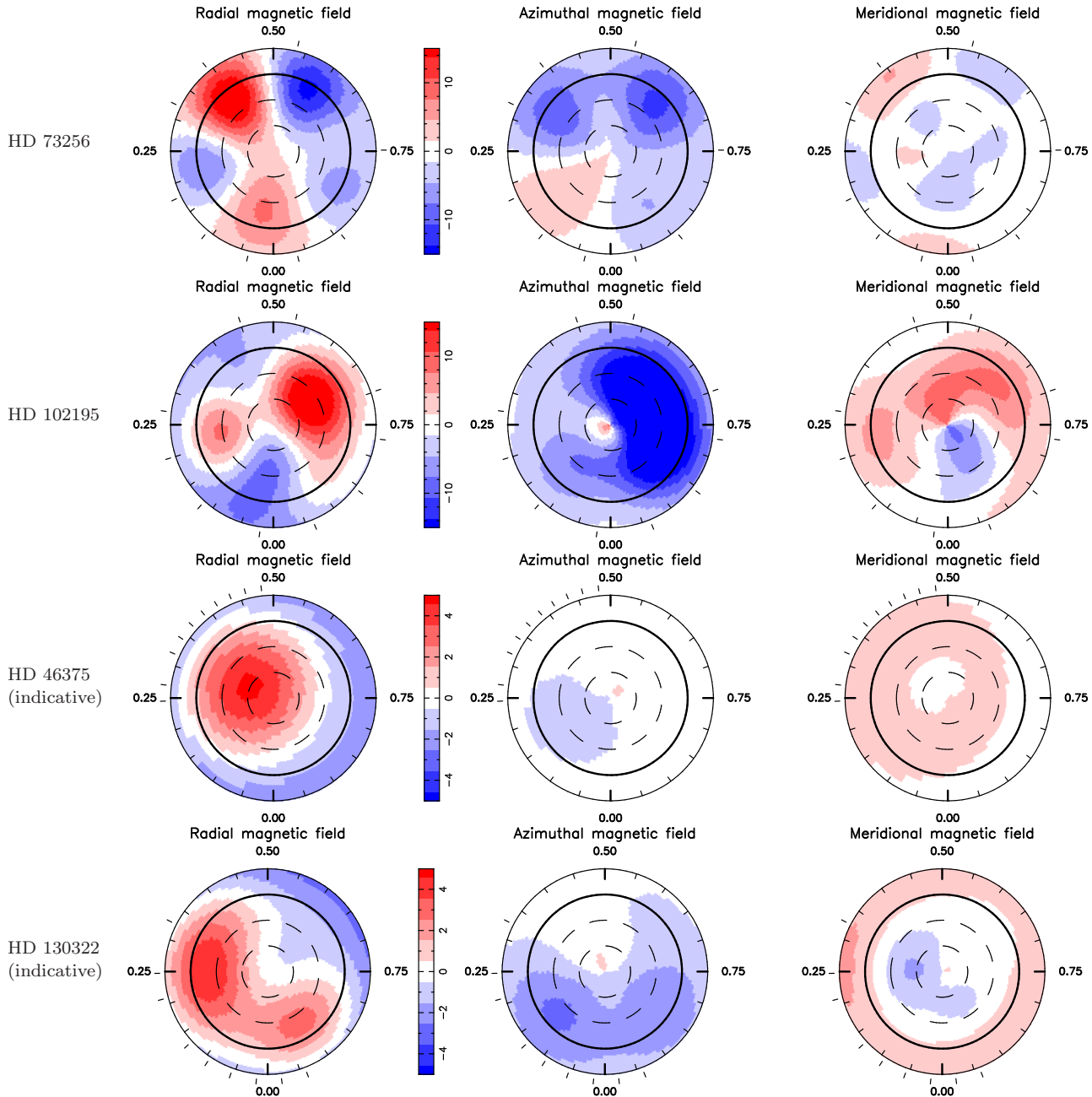


**Figure 5.** Magnetic maps of HD 73256, HD 102195, HD 46375 and HD 130322 from top to bottom rows. See legend details in Figure 5.

2008 with ESPaDOnS (Figure 4 third column) are compatible with a dipole observed partially and also correspond to a dipole of a few G amplitude. We cannot however constrain the dipole tilt nor get a high confidence on the mean magnetic strength of the large-scale structure. The map given in Figure 5 (third row) is indicative and fairly similar to the one obtained by Gaulme et al. (2010).

#### 4.5 HD 130322

Nine ESPaDOnS spectra of HD 130322 (K0V) were secured in January 2008. The rotation period of this star is 26 days (Simpson et al. 2010), much longer than our observing run of 10 days. As a consequence, only one third of the stellar

surface is observed. This makes difficult a full reconstruction of the magnetic topology, since we do not have observational constraints on the un-observed part of the star (see Appendix B in Fares et al. (2012)). The circular polarisation profiles are, however, significantly detected in all observing epochs.

We adopted a value of  $80^\circ$  for the stellar inclination and reconstruct the map with a  $\chi_r^2$  of 0.9 (Fig. 5 fourth row). The circular polarisation profiles (Fig 4, fourth column) are well-fitted by a magnetic structure dominated by a dipole (only  $\sim 16\%$  of the field energy is toroidal) of 2.5 G mean strength. Data over more than a full rotation period would be needed to confirm this result and could still reveal a more complex large-scale structure of the magnetic field.

#### 4.6 HD 189733

Table 1 includes three observational campaigns of HD 189733 (K2V) using ESPaDOnS and NARVAL in 2006, 2007 and 2008 for completion with respect to the target sample presented here. However, their analysis has already been published in Moutou et al. (2007) and Fares et al. (2010) and will not be repeated here. HD 189733 has a mainly toroidal surface magnetic field with a strength of 20 to 40 G. The stellar surface has a DR of  $d\Omega = 0.146 \pm 0.049 \text{ rad d}^{-1}$ . The field extrapolation up to the location of the planet has been derived by Fares et al. (2009) and Cohen et al. (2011). The planet is found to cross different stellar field configurations along its orbit. This makes the reconnection events between stellar and planetary magnetic fields possible on fractions of the orbit. The planetary radio emission from magnetospheric interaction with the stellar wind varies along the orbit (Fares et al. 2010)

#### 4.7 HD 179949

Two epochs of ESPaDOnS observations of HD 179949 (F8V) have been discussed in Fares et al. (2012). The 2009 data set is part of a joined campaign with XMM and ground-based spectroscopic data taken simultaneously with the spectropolarimetric observations. The additional data are described in Scandariato et al. (2013). HD 179949 exhibits a weak and mainly poloidal magnetic field of a few G and a tilt of  $\sim 70^\circ$ . A DR of  $d\Omega = 0.216 \pm 0.061 \text{ rad d}^{-1}$  has been measured. In this case also, the field at the stellar surface has been extrapolated up to the planetary orbit, for further studies concerning modelling the interactions (Fares et al. 2012).

#### 4.8 Stars without detected fields

##### *XO-3*

We have secured twenty independent observations of XO-3 (F5V) with ESPADONS in October 2009. Despite a high SNR for most spectra (12 out of 20 have SNR above  $\sim 300$ ), there was no detection of polarisation in the Stokes V profiles.

In order to quantify an upper limit for a magnetic field of XO-3, we propose the following analysis:

(i) We select a star with similar mass and a rotation period to XO-3, but for which we have a magnetic field detection. The reconstructed magnetic field of the chosen star is used as a magnetic topology model for XO-3.

(ii) From this fake magnetic field, we calculate Stokes V profiles. We compare these profiles to the observed noise properties at the phases of our observations.

(iii) If the signal exceeds the noise and should have led to a detection, we decrease the field strength, without changing its topology. We repeat step 2 until the signal from the fake Stokes V profile is just about the noise level of the observations, at which a lower limit on the magnetic field of the star is derived.

This analysis may give a reasonable order of magnitude of the maximum field strength excluded by our data for a chosen field topology. It must be noted, however, that other parameters may alter this value as the inclination (low

impact), the temporal sampling of the observations and the field complexity. This attempt to quantify our non-detection should therefore not be over-interpreted.

In the case of XO-3 where we have numerous observations and a fast rotating star ( $v \sin i = 18.3 \text{ km s}^{-1}$ ), the detection limit has the most relevant significance. We injected signals corresponding to two stars where a magnetic topology has been deduced from previous observations, and relatively close in stellar properties to XO-3: HD 102195 (section 4.3) and HD 179949 (Fares et al. 2012). HD 179949 has an effective temperature close to that of XO-3 but has a Rossby number  $> 1.0$ , while HD 102195 has a lower mass than XO-3 but has, as XO-3, a Rossby number  $< 1.0$  (magnetic fields show similar properties for stars in different Rossby regimes, see section 5). A field with similar properties than HD 102195 (with a mean field strength  $\sim 10 \text{ G}$ ) projected on the observation space of XO-3 remains undetected at  $3\sigma$  except in one spectrum and represents a reasonable detection limit in the context of a HD 102195's 55% toroidal magnetic field topology. The field of HD 179949, as characterized from the 2009 ESPaDOnS campaign (Fares et al. 2012) is undetectable in the signal of XO-3. We multiplied by 10 all components of this magnetic field and found that the fake Stokes V signatures would have been detected in 7 over the 15 best-quality spectra with a significance larger than  $3\sigma$ . Thus, a mostly (90%) poloidal field with an amplitude of 20 G would have been unambiguously detected. We adopt this more conservative value for an upper limit for the magnetic field strength of XO-3 during the 2009 observation campaign.

##### *HAT-P-2 = HD 147506*

HAT-P-2 (F8) has been observed four times between 26 June and 1 July 2007. None of the spectra shows a detection of the magnetic field, with a mean rms noise level in the LSD profiles of  $0.5 \times 10^{-4}$ . HAT-P-2 is a fast rotating star with an effective temperature of 6290K, so its properties closely match the ones of  $\tau$  Boo. In order to investigate the detection limit of the magnetic field in our data, we thus used one of the magnetic configurations depicted for  $\tau$  Boo, scaled the field strength and calculated the fake Stokes V signatures that would have been produced at our observing sampling. We find that a 75% poloidal field of 40 G would have been detected in two over the four observed phases. The actual field is thus either of very different configuration, or of lower strength (or both).

##### *CoRoT-7*

Four spectra of CoRoT-7 (G9V) have been secured with NARVAL in January 2010. Due to the faint luminosity of the star (V magnitude=11.7), the field detection represents a real challenge, especially for NARVAL. The SNR of the profiles is ten times lower than for HAT-P-2. In all four spectra, there is a spurious detection in the Stokes V profile, also detected in the null-polarisation check profiles. Only the last exposure shows a marginal detection of the magnetic field, with a Stokes V profile slightly larger than the null profile. We applied the same strategy described for XO-3 and HAT-P-2, taking a dipole as the magnetic model for this



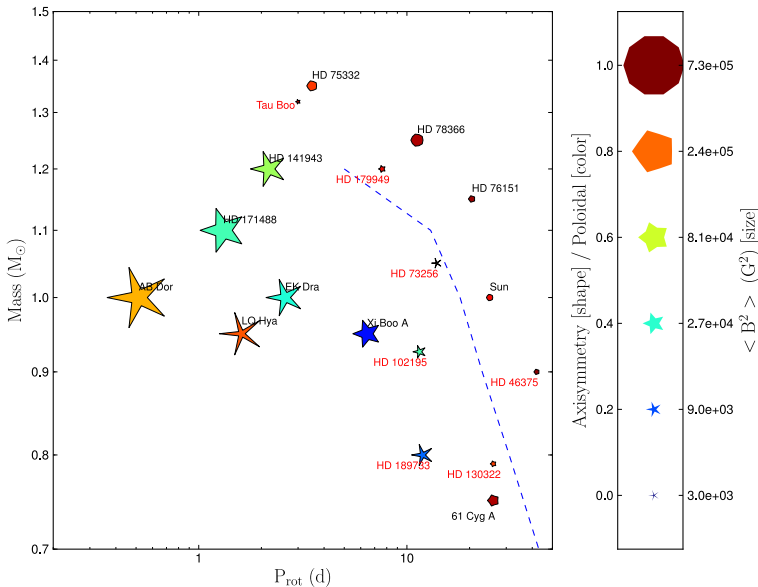


**Figure 6.** Mass-rotation diagram of 18 reconstructed stellar magnetic fields (not including dM stars for instance). Planet host stars studied in this paper have their names indicated in red, while other stars without detected hot Jupiters have their names indicated in black (data from Donati & Landstreet (2009)). The dashed line represent Rossby number = 1.0 (calculated using results of Landin, Mendes & Vaz (2010)). The size of the symbol represents the field strength, its color the contribution of the poloidal component to the field, and its shape how axisymmetric the poloidal component is. For  $\tau$  Boo, we show here the field for one epoch of observation (mainly poloidal). Hot-Jupiter host stars do not seem to have different magnetic properties than the other stars.

star (similar to the topology of HD 46375). We compared the fake Stokes V signatures that a dipolar field would produce at our observing phases. We find that a dipole with more than 150G strength would have been significantly detected in two spectra over the four available ones, and beyond the marginal detection on 27 January 2008. The detection limit represents a poorer constraint than for XO-3 and HAT-P-2, because the star is of lower mass, a slower rotator, and the spectra have lower SNR.

## 5 DISCUSSION AND SUMMARY

A summary of the main characteristics of the stellar magnetic fields observed in this study is given in Table 1. When the field is not detected, the upper value derived as explained above is shown. The stars of this study, with stellar masses 0.8 to 1.4  $M_{\odot}$ , feature large-scale magnetic fields of 2 to 40 G. Except at two epochs for HD 189733 and HD 102195, all other targets have mainly poloidal fields, with varying degrees of axisymmetry.

The presence of a giant planet at a small orbital distance is thought to have influences on the star. Empirical evidence suggest that tidal interactions can cause excess rotation of the parent star (Pont 2009). Cuntz et al. (2000) suggest that these interactions can cause local instabilities

in the tidal bulges and thus modify the local dynamo on action in these regions. Cebron et al. (011a,b) present theoretical work on the effect of tidally-driven elliptical instability on star hosting a hot-Jupiter (HJ) and suggest that eventually these instabilities can produce a dynamo. In order to study possible peculiarities in the magnetic topologies of HJ host stars, one should compare their magnetic topologies to that of similar stars without detected closed-in giant planets. Figure 6 shows a mass-rotation plane including the magnetic properties of stars of our sample (whose names are shown in red), as well as other published stellar field properties (from Donati & Landstreet 2009). A main transition appears in this plot for stars with masses above 0.5  $M_{\odot}$ : i) below Rossby number of  $\sim 1$ , the large-scale field is mainly toroidal, with a non-axisymmetric poloidal component; ii) above Rossby number of  $\sim 1$ , the field is weaker, poloidal and axisymmetric. The long-term evolution of the magnetic fields should however be taken into account, with possible cycles, as for the Sun and a few other known examples (Donati et al. 2008; Fares et al. 2009; Morgenthaler et al. 2011). Our HJ host stars show similar field topologies as the stars without a discovered close-in giant planet. The strength of their magnetic fields seems weaker, however, our sample is basically of stars chosen for radial velocity studies, they are less active than the other stars shown in Figure 6. In addition, if the data quality is poor (poor S/N and poor phase coverage), the reconstructed magnetic field strength is reduced below what would be reconstructed with higher quality data (see Fares et al. 2012). In order to comment of the field strength of planet-host stars, it is necessary to enlarge our sample.

$\tau$  Boo’s magnetic cycle is confirmed to be a short one. Observed between June 2006 and January 2011, the large-scale magnetic field of this star switches polarity yearly. However, the cycle duration might be of 2 years or of 8 months, as both periods are good solutions for the data we have. In the frequency domain, the 240 day period is the third harmonic of the 740 day period. The period of 740 days seems more likely. Previous studies of the chromospheric activity of this star found a period of 126 days persistent over 30 years (Maulik et al. 1997; Baliunas et al. 1997). If the relation between the activity cycle to the large-scale magnetic field cycle in stars is similar to that of the Sun, this favours the 8 month period for the magnetic cycle. However, such a relation is not known for stars (there is a lack of observed large-scale magnetic cycles), and thus it can not help us rule out one of the the two values we get. In order to favor one value over the other, we suggest dense observations of this star over a year, with at least 4 epochs of observations. Constraining the period will permit a comparison with the solar chromospheric/magnetic cycle behaviour.

Poppenhaeger et al. (2012) observed  $\tau$  Boo in X-rays over six epochs (one observation in June 2003 and then 5 between June 2010 and June 2011). The star shows variability in X-rays, but a cyclic behaviour was not observed. They conjecture that the lack of X-ray cycles could be explained by either their sparse sampling, or that the polarity switch could be an artificial feature from the reconstruction method (ZDI) rather than being a real polarity switch. We note however that the lack of X-ray cycle does not rule out the presence of polarity switches (magnetic cycles), as have been predicted by theoretical works (McIvor et al. 006b, see

also Baumann et al. 2004; Işık et al. 2011). Furthermore, in the particular case of  $\tau$  Boo, Vidotto et al. (2012) simulated its stellar wind through the magnetic cycle, and studied mass-loss and angular-momentum loss rates, as well as X-ray emission measure and planetary radio emission. In their study, they used the magnetic maps from Fares et al. 2009; Donati et al. 2008; Catala et al. 2007 as boundary condition for the stellar magnetic field (they thus considered the polarity switch in their model). They find that the emission measure does not vary during the cycle, suggesting that the quiescent X-ray emission of  $\tau$  Boo does not change significantly over the cycle, agreeing with the findings of Poppenhaeger et al. (2012).

The goal of this work is to study for the first time the magnetic fields of a sample of planet-host stars. When possible, we reconstructed the stellar magnetic fields. We found a wide range of topologies. In order to check if these topologies are peculiar, we compared them to those of stars without detected hot-Jupiters. We found that these planet-host stars do not show peculiar magnetic behaviours. Our study shows that the stellar magnetic field topology is usually more complex than a simple dipole or quadrupole. Thus, it is essential to use the reconstructed maps in simulations (instead of modelling the field by a simple dipole). Our work is thus a basis for future star-planet interactions simulations, wind models, and simulations of radio and X-ray emission. We will make our magnetic maps available to the public on the following link <http://lamwws.oamp.fr/exo/starplanetinteractions/mtphs>.

## ACKNOWLEDGMENTS

RF acknowledges support from STFC consolidated grant ST/J001651/1. This work is based on observations obtained with ESPaDOnS at the Canada-France-Hawaii Telescope (CFHT) and with NARVAL at the T lescope Bernard Lyot (TBL). CFHT/ESPaDOnS are operated by the National Research Council of Canada, the Institut National des Sciences de l'Univers of the Centre National de la Recherche Scientifique (INSU/CNRS) of France, and the University of Hawaii, while TBL/NARVAL are operated by INSU/CNRS. We thank the CFHT and TBL staff for their help during the observations. We thank an anonymous referee for their comments.

## REFERENCES

- Baliunas S. L., Henry G. W., Donahue R. A., Fekel F. C., Soon W. H., 1997, *ApJL*, 474, L119
- Baumann I., Schmitt D., Sch ssler M., Solanki S. K., 2004, *A&A*, 426, 1075
- Bouchy F., Udry S., Mayor M., Moutou C., Pont F., Iribarne N., da Silva R., Ilovaisky S., Queloz D., Santos N., S gransan D., Zucker S., 2005, *A&A*, 444, L15
- Broggi M., Snellen I. A. G., de Kok R. J., Albrecht S., Birkby J., de Mooij E. J. W., 2012, *Nature*, 486, 502
- Bruntt H., Deleuil M., Fridlund M., Alonso R., Bouchy F., Hatzes A., Mayor M., Moutou C., Queloz D., 2010, *A&A*, 519, A51
- Butler R. P., Wright J. T., Marcy G. W., Fischer D. A., Vogt S. S., Tinney C. G., Jones H. R. A., Carter B. D., Johnson J. A., McCarthy C., Penny A. J., 2006, *ApJ*, 646, 505
- Catala C., Donati J.-F., Shkolnik E., Bohlender D., Alecian E., 2007, *MNRAS*, 374, L42
- Cebron D., Le Bars M., Moutou C., Maubert P., Le Gal P., 2011b, in *EPSC-DPS Joint Meeting 2011 Tides induced magnetic field in the solar system*. p. 1080
- Cebron D., Moutou C., Le Bars M., Le Gal P., Far s R., 2011a, in *European Physical Journal Web of Conferences Vol. 11 of European Physical Journal Web of Conferences*, Tidal instability in exoplanetary systems evolution. p. 3003
- Cohen O., Drake J. J., Kashyap V. L., Sokolov I. V., Gombosi T. I., 2010, *ApJL*, 723, L64
- Cohen O., Kashyap V. L., Drake J. J., Sokolov I. V., Garraffo C., Gombosi T. I., 2011, *ApJ*, 733, 67
- Cranmer S. R., Saar S. H., 2007, *ArXiv Astrophysics e-prints*, p. 0702530
- Cuntz M., Saar S. H., Musielak Z. E., 2000, *ApJ*, 533, L151
- Dobbs-Dixon I., Lin D. N. C., Mardling R. A., 2004, *ApJ*, 610, 464
- Donati J.-F., Howarth I., Jardine M., Petit P., Catala C., Landstreet J., Bouret J., Alecian E., Barnes J., Forveille T., Paletou F., Manset N., 2006, *MNRAS*, 370, 629
- Donati J.-F., Landstreet J. D., 2009, *ARA&A*, 47, 333
- Donati J.-F., Moutou C., Far s R., Bohlender D., Catala C., Deleuil M., Shkolnik E., Cameron A. C., Jardine M. M., Walker G. A. H., 2008, *MNRAS*, 385, 1179
- Donati J.-F., Semel M., Carter B. D., Rees D. E., Collier Cameron A., 1997, *MNRAS*, 291, 658
- Fares R., Donati J.-F., Moutou C., Bohlender D., Catala C., Deleuil M., Shkolnik E., Collier Cameron A., Jardine M. M., Walker G. A. H., 2009, *MNRAS*, 398, 1383
- Fares R., Donati J.-F., Moutou C., Jardine M., Cameron A. C., Lanza A. F., Bohlender D., Dieters S., Mart nez Fiorenzano A. F., Maggio A., Pagano I., Shkolnik E. L., 2012, *MNRAS*, 423, 1006
- Fares R., Donati J.-F., Moutou C., Jardine M. M., Gri smeier J.-M., Zarka P., Shkolnik E. L., Bohlender D., Catala C., Collier Cameron A., 2010, *MNRAS*, 406, 409
- Gaulme P., Deheuvels S., Weiss W. W., Mosser B., Moutou C., Bruntt H., Donati J.-F., Vannier M., Guillot T., Appourchaux T., Michel E., Auvergne M., Samadi R., Baudin F., Catala C., Baglin A., 2010, *A&A*, 524, A47
- Ge J., van Eyken J., Mahadevan S., DeWitt C., Kane S. R., Cohen R., 2006, *ApJ*, 648, 683
- Işık E., Schmitt D., Sch ssler M., 2011, *A&A*, 528, A135
- Jardine M., Collier Cameron A., Donati J.-F., 2002, *MNRAS*, 333, 339
- Johns-Krull C. M., McCullough P. R., Burke C. J., Valenti J. A., Janes K. A., Heasley J. N., Prato L., Bissinger R., Fleenor M., Foote C. N., Garcia-Melendo E., Gary B. L., Howell P. J., Mallia F., Masi G., Vanmunster T., 2008, *ApJ*, 677, 657
- Lai D., Foucart F., Lin D. N. C., 2011, *MNRAS*, 412, 2790
- Landin N. R., Mendes L. T. S., Vaz L. P. R., 2010, *A&A*, 510, A46
- Lanza A. F., 2012, *A&A*, 544, A23
- L ger A., Rouan D., Schneider J., Barge P., Fridlund M., Samuel B., Ollivier M., Guenther E., Deleuil M., Deeg

- H. J., Auvergne M., Alonso R., Aigrain S., Alapini A., Almenara J. M., Baglin A., 2009, *A&A*, 506, 287
- Maulik D., Donahue R. A., Baliunas S. L., 1997, Technical report, Persistent Sub-Yearly Chromospheric Variations in Lower Main-Sequence Stars: Tau Booe and alpha COM
- McIvor T., Jardine M., Mackay D., Holzwarth V., 2006b, *MNRAS*, 367, 592
- Melo C., Santos N. C., Gieren W., Pietrzynski G., Ruiz M. T., Sousa S. G., Bouchy F., Lovis C., Mayor M., Pepe F., Queloz D., da Silva R., Udry S., 2007, *A&A*, 467, 721
- Morgenthaler A., Petit P., Morin J., Aurière M., Dintrans B., Konstantinova-Antova R., Marsden S., 2011, *Astronomische Nachrichten*, 332, 866
- Morin J., Donati J.-F., Petit P., Delfosse X., Forveille T., Albert L., Aurière M., Cabanac R., Dintrans B., Fares R., Gastine T., shk08 M. M., Lignières F., Paletou F., Ramirez Velez J. C., Théado S., 2008, *MNRAS*, 390, 567
- Moutou C., Donati J.-F., Savalle R., Hussain G., Alecian E., Bouchy F., Catala C., Collier Cameron A., Udry S., Vidal-Madjar A., 2007, *A&A*, 473, 651
- Pagano I., Lanza A. F., Leto G., Messina S., Barge P., Baglin A., 2009, *Earth Moon and Planets*, 105, 373
- Pál A., Bakos G. Á., Torres G., Noyes R. W., Fischer D. A., Johnson J. A., Henry G. W., Butler R. P., Marcy G. W., Howard A. W., Sipőcz B., Latham D. W., Esquerdo G. A., 2010, *MNRAS*, 401, 2665
- Pont F., 2009, *MNRAS*, 396, 1789
- Poppenhaeger K., Günther H. M., Schmitt J. H. M. M., 2012, *Astronomische Nachrichten*, 333, 26
- Rodler F., Kürster M., López-Morales M., Ribas I., 2013, *Astronomische Nachrichten*, 334, 188
- Scandariato G., Maggio A., Lanza A. F., Pagano I., Fares R., Shkolnik E. L., Bohlender D., Cameron A. C., Dieters S., Donati J.-F., Martínez Fiorenzano A. F., Jardine M., Moutou C., 2013, *A&A*, 552, A7
- Shkolnik E., Bohlender D. A., Walker G. A. H., Collier Cameron A., 2008, *ApJ*, 676, 628
- Shkolnik E., Walker G., Bohlender D., 2003, *ApJ*, 597, 1092
- Shkolnik E., Walker G., Bohlender D., Gu P., Kürster M., 2005, *ApJ*, 622, 1075
- Simpson E. K., Baliunas S. L., Henry G. W., Watson C. A., 2010, *MNRAS*, 408, 1666
- Udry S., Mayor M., Clausen J. V., Freyhammer L. M., Helt B. E., Lovis C., Naef D., Olsen E. H., Pepe F., Queloz D., Santos N. C., 2003, *A&A*, 407, 679
- Udry S., Mayor M., Naef D., Pepe F., Queloz D., Santos N. C., Burnet M., Confino B., Melo C., 2000, *A&A*, 356, 590
- Vidotto A. A., Fares R., Jardine M., Donati J.-F., Opher M., Moutou C., Catala C., Gombosi T. I., 2012, *MNRAS*, 423, 3285
- Walker G. A. H., Croll B., Matthews J. M., Kuschnig R., Huber D., Weiss W. W., Shkolnik E., Rucinski S. M., Guenther D. B., Moffat A. F. J., Sasselov D., 2008, *A&A*, 482, 691
- Winn J. N., Johnson J. A., Fabrycky D., Howard A. W., Marcy G. W., Narita N., Crossfield I. J., Suto Y., Turner E. L., Esquerdo G., Holman M. J., 2009, *ApJ*, 700, 302

## APPENDIX A: JOURNAL OF OBSERVATIONS

In this Appendix, the detailed journal of observations (Tables A1, A2 and A3) is given for all data of the survey, except the ones already published in Catala et al. (2007); Donati et al. (2008); Moutou et al. (2007); Fares et al. (2009, 2010, 2012).

**Table A1.** Journal of observations of  $\tau$  Boo. Columns 1–12 sequentially list the star name, UT date, instrument used, the heliocentric Julian date (at mid-exposure), the UT time (at mid-exposure), the complete exposure time, the peak signal to noise ratio (per  $2.6 \text{ km s}^{-1}$  velocity bin) of each observation (around  $700 \text{ nm}$ ), the rotational cycle, the radial velocity (RV) associated with each exposure, the rms noise level (relative to the unpolarized continuum level  $I_c$  and per  $1.8 \text{ km s}^{-1}$  velocity bin) in the circular polarisation profile produced by Least-Squares Deconvolution (LSD), the longitudinal magnetic field and the false-alarm probability of the detection of the magnetic signature.

Star	Date	Instrument	HJD (245 4000+)	UT (h:m:s)	$T_{exp}$ (s)	S/N	$\phi_{rot}$	RV ( $\text{km s}^{-1}$ )	$\sigma_{LSD}$ ( $10^{-4} I_c$ )	$B_l$ (G)	FAP
$\tau$ Boo	27may09	Narval	979.39142	21:18:08	$4 \times 700$	1030	-2.531	-16.163	0.33	$-0.0 \pm 1.5$	$3.279 \times 10^{-01}$
$\tau$ Boo	27may09	Narval	979.44073	22:29:08	$4 \times 700$	1410	-2.514	-16.189	0.25	$-0.7 \pm 1.1$	$5.612 \times 10^{-01}$
$\tau$ Boo	27may09	Narval	979.55991	01:20:46	$4 \times 600$	1430	-2.475	-16.276	0.27	$0.2 \pm 1.2$	$8.699 \times 10^{-01}$
$\tau$ Boo	28may09	Narval	980.40258	21:34:17	$4 \times 700$	1650	-2.194	-16.821	0.22	$-0.4 \pm 1.0$	$6.172 \times 10^{-01}$
$\tau$ Boo	28may09	Narval	980.43825	22:25:39	$4 \times 700$	1710	-2.182	-16.832	0.22	$-0.6 \pm 1.0$	$9.594 \times 10^{-01}$
$\tau$ Boo	29may09	Narval	981.47684	23:21:18	$4 \times 700$	1500	-1.836	-16.278	0.26	$1.0 \pm 1.2$	$5.935 \times 10^{-07}$
$\tau$ Boo	31may09	Narval	983.56341	01:26:07	$4 \times 700$	1880	-1.140	-16.813	0.19	$0.4 \pm 0.9$	$8.525 \times 10^{-01}$
$\tau$ Boo	01jun09	Narval	984.38396	21:07:46	$4 \times 700$	1880	-0.867	-16.643	0.19	$-1.8 \pm 0.8$	$2.259 \times 10^{-11}$
$\tau$ Boo	01jun09	Narval	984.41875	21:57:52	$4 \times 700$	1830	-0.855	-16.620	0.19	$-0.8 \pm 0.9$	$5.689 \times 10^{-06}$
$\tau$ Boo	02jun09	Narval	985.36661	20:42:52	$4 \times 700$	1800	-0.539	-15.948	0.19	$0.8 \pm 0.8$	$7.379 \times 10^{-02}$
$\tau$ Boo	02jun09	Narval	985.40138	21:32:56	$4 \times 700$	1880	-0.527	-15.951	0.19	$1.6 \pm 0.8$	$1.343 \times 10^{-08}$
$\tau$ Boo	11jun09	Narval	994.40998	21:46:06	$4 \times 700$	1380	2.475	-16.520	0.26	$1.2 \pm 1.2$	$6.621 \times 10^{-01}$
$\tau$ Boo	11jun09	Narval	994.44475	22:36:11	$4 \times 700$	1380	2.487	-16.484	0.28	$1.4 \pm 1.3$	$4.310 \times 10^{-01}$
$\tau$ Boo	12jun09	Narval	995.39500	21:24:37	$4 \times 700$	1360	2.804	-15.935	0.30	$-1.7 \pm 1.3$	$2.871 \times 10^{-02}$
$\tau$ Boo	12jun09	Narval	995.42978	22:14:42	$4 \times 700$	1480	2.815	-15.923	0.28	$-1.9 \pm 1.2$	$8.053 \times 10^{-03}$
$\tau$ Boo	15jun09	Narval	998.54978	01:07:48	$4 \times 600$	1690	3.855	-15.940	0.24	$-2.3 \pm 1.1$	$8.522 \times 10^{-01}$
$\tau$ Boo	25jan10	Narval	1222.66429	03:55:40	$4 \times 600$	1730	-3.147	-16.860	0.20	$-1.2 \pm 0.9$	$8.225 \times 10^{-07}$
$\tau$ Boo	25jan10	Narval	1222.73534	05:37:58	$4 \times 600$	1790	-3.126	-16.837	0.19	$-2.3 \pm 0.9$	$8.424 \times 10^{-11}$
$\tau$ Boo	25jan10	Narval	1222.76651	06:22:52	$4 \times 600$	1590	-3.116	-16.825	0.22	$-0.6 \pm 1.0$	$2.225 \times 10^{-06}$
$\tau$ Boo	27jan10	Narval	1224.64686	03:30:20	$4 \times 600$	1660	-2.549	-16.300	0.22	$2.5 \pm 1.0$	$6.221 \times 10^{-05}$
$\tau$ Boo	27jan10	Narval	1224.71461	05:07:53	$4 \times 600$	1490	-2.528	-16.361	0.24	$2.9 \pm 1.1$	$3.485 \times 10^{-02}$
$\tau$ Boo	12feb10	Narval	1240.59580	02:14:58	$4 \times 600$	1260	2.266	-16.041	0.34	$1.0 \pm 1.5$	$5.891 \times 10^{-01}$
$\tau$ Boo	13feb10	Narval	1241.63537	03:11:51	$4 \times 600$	1020	2.580	-16.747	0.43	$-1.0 \pm 1.9$	$6.981 \times 10^{-01}$
$\tau$ Boo	13feb10	Narval	1241.71688	05:09:13	$4 \times 600$	1130	2.605	-16.813	0.37	$-2.2 \pm 1.7$	$4.960 \times 10^{-02}$
$\tau$ Boo	14feb10	Narval	1242.60430	02:26:60	$4 \times 600$	1570	2.872	-16.833	0.23	$1.2 \pm 1.0$	$7.482 \times 10^{-05}$
$\tau$ Boo	14feb10	Narval	1242.71737	05:09:49	$4 \times 600$	1630	2.907	-16.737	0.21	$-0.4 \pm 0.9$	$5.608 \times 10^{-09}$
$\tau$ Boo	14jan11	Narval	1576.70136	04:50:25	$4 \times 600$	1730	-2.267	-16.956	0.19	$1.1 \pm 0.9$	$9.118 \times 10^{-04}$
$\tau$ Boo	15jan11	Narval	1577.69079	04:35:04	$4 \times 600$	1490	-1.968	-16.357	0.23	$-0.4 \pm 1.0$	$1.731 \times 10^{-03}$
$\tau$ Boo	16jan11	Narval	1578.68566	04:27:34	$4 \times 600$	1840	-1.668	-16.057	0.18	$-0.4 \pm 0.8$	$2.920 \times 10^{-01}$
$\tau$ Boo	22jan11	Narval	1584.67961	04:18:07	$4 \times 600$	1670	0.142	-16.147	0.20	$-1.4 \pm 0.9$	$5.847 \times 10^{-01}$
$\tau$ Boo	22jan11	Narval	1584.70997	05:01:50	$4 \times 600$	1660	0.151	-16.126	0.20	$-0.9 \pm 0.9$	$8.562 \times 10^{-02}$
$\tau$ Boo	22jan11	Narval	1584.74032	05:45:32	$4 \times 600$	1530	0.160	-16.117	0.22	$-1.7 \pm 1.0$	$6.900 \times 10^{-01}$
$\tau$ Boo	23jan11	Narval	1585.68804	04:30:08	$4 \times 600$	1760	0.446	-16.390	0.18	$0.8 \pm 0.8$	$3.481 \times 10^{-03}$
$\tau$ Boo	23jan11	Narval	1585.72592	05:24:41	$4 \times 600$	1860	0.458	-16.428	0.18	$-0.3 \pm 0.8$	$2.009 \times 10^{-03}$
$\tau$ Boo	23jan11	Narval	1585.75629	06:08:24	$4 \times 600$	1810	0.467	-16.450	0.18	$1.7 \pm 0.8$	$2.857 \times 10^{-05}$
$\tau$ Boo	24jan11	Narval	1586.66487	03:56:39	$4 \times 600$	1580	0.741	-17.000	0.23	$-0.3 \pm 1.0$	$2.588 \times 10^{-03}$
$\tau$ Boo	24jan11	Narval	1586.695230	04:40:22	$4 \times 600$	1700	0.750	-16.995	0.20	$-0.7 \pm 0.9$	$8.092 \times 10^{-03}$
$\tau$ Boo	24jan11	Narval	1586.725580	05:24:05	$4 \times 600$	1790	0.759	-16.993	0.19	$0.5 \pm 0.8$	$9.390 \times 10^{-03}$
$\tau$ Boo	25jan11	Narval	1587.666570	03:58:59	$4 \times 600$	1780	1.043	-16.391	0.18	$0.3 \pm 0.8$	$3.947 \times 10^{-01}$
$\tau$ Boo	25jan11	Narval	1587.696930	04:42:42	$4 \times 600$	1830	1.053	-16.362	0.18	$-0.9 \pm 0.8$	$9.800 \times 10^{-02}$
$\tau$ Boo	25jan11	Narval	1587.727280	05:26:24	$4 \times 600$	1820	1.062	-16.336	0.18	$-0.4 \pm 0.8$	$8.442 \times 10^{-03}$
$\tau$ Boo	26jan11	Narval	1588.674650	04:10:30	$4 \times 600$	930	1.348	-16.197	0.37	$2.8 \pm 1.6$	$5.712 \times 10^{-01}$
$\tau$ Boo	26jan11	Narval	1588.705000	04:54:12	$4 \times 600$	1190	1.357	-16.211	0.28	$0.0 \pm 1.2$	$4.340 \times 10^{-01}$
$\tau$ Boo	26jan11	Narval	1588.735360	05:37:55	$4 \times 600$	1650	1.366	-16.227	0.20	$-0.4 \pm 0.9$	$5.440 \times 10^{-02}$

**Table A2.** Journal of observations of four stars for which the magnetic field was detected and analysed.

Star	Date	Instrument	HJD (245 4000+)	UT time (h:m:s)	$T_{exp}$ (s)	S/N	$\phi_{rot}$	RV ( $\text{km s}^{-1}$ )	$\sigma_{LSD}$ ( $10^{-4}I_c$ )	$B_l$ (G)	FAP
HD 73256	19jan08	ESPaDOnS	484.89743	09:24:56	4×560	410	-0.252	30.322	0.78	-2.6±1.5	$8.171 \times 10^{-3}$
HD 73256	21jan08	ESPaDOnS	486.89575	09:22:25	4×560	540	-0.109	29.997	0.56	1.0±1.1	$9.523 \times 10^{-1}$
HD 73256	22jan08	ESPaDOnS	487.91245	09:46:26	4×560	600	-0.036	30.313	0.51	5.3±1.0	$< 10^{-8}$
HD 73256	23jan08	ESPaDOnS	488.95053	10:41:13	4×700	540	0.038	29.858	0.57	4.2±1.1	$< 10^{-8}$
HD 73256	24jan08	ESPaDOnS	489.94860	10:38:24	4×780	700	0.109	30.302	0.43	0.5±0.9	$1.836 \times 10^{-6}$
HD 73256	25jan08	ESPaDOnS	490.90682	09:38:12	4×630	580	0.178	30.050	0.53	-1.4±1.1	$9.917 \times 10^{-2}$
HD 73256	27jan08	ESPaDOnS	492.91695	09:52:43	4×900	580	0.321	30.356	0.47	0.3±0.9	$< 10^{-8}$
HD 73256	28jan08	ESPaDOnS	493.91923	09:55:58	4×900	390	0.393	29.877	0.69	4.6±1.4	$< 10^{-8}$
HD 73256	30jan08	ESPaDOnS	495.92900	10:09:58	2×900	360	0.536	30.131	0.83	-0.7±1.6	$< 10^{-8}$
HD 102195	19jan08	ESPaDOnS	484.95747	10:54:30	4×540.0	270	-0.228	2.209	1.31	5.4±2.4	$< 10^{-8}$
HD 102195	20jan08	ESPaDOnS	485.95843	10:55:46	4×560.0	620	-0.145	2.112	0.51	6.3±1.0	$< 10^{-8}$
HD 102195	21jan08	ESPaDOnS	486.95369	10:48:49	4×560.0	560	-0.062	2.132	0.57	5.5±1.2	$< 10^{-8}$
HD 102195	22jan08	ESPaDOnS	487.94096	10:30:22	4×560.0	620	0.020	2.142	0.51	2.6±1.1	$5.1 \times 10^{-5}$
HD 102195	23jan08	ESPaDOnS	489.09831	14:16:50	4×780.0	680	0.117	2.101	0.46	2.2±0.9	$2.1 \times 10^{-1}$
HD 102195	24jan08	ESPaDOnS	490.10308	14:23:34	4×630.0	610	0.200	2.028	0.51	3.6±1.1	$1.3 \times 10^{-5}$
HD 102195	25jan08	ESPaDOnS	490.93814	10:25:58	4×630.0	500	0.270	2.119	0.65	3.3±1.3	$3.4 \times 10^{-2}$
HD 102195	27jan08	ESPaDOnS	493.10187	14:21:30	4×700.0	640	0.450	2.137	0.45	-1.1±0.8	$6.6 \times 10^{-3}$
HD 102195	28jan08	ESPaDOnS	494.10213	14:21:46	4×700.0	590	0.533	2.013	0.48	0.7±1.0	$5.1 \times 10^{-6}$
HD 102195	30jan08	ESPaDOnS	496.09029	14:04:31	4×800.0	440	0.699	2.164	0.63	5.5±1.3	$< 10^{-8}$
HD 46375	18jan08	ESPaDOnS	483.84291	08:06:50	4×215	460	0.245	-0.910	0.68	2.1±0.9	$< 10^{-8}$
HD 46375	19jan08	ESPaDOnS	484.83247	07:51:51	4×560	550	0.269	-0.912	0.56	2.4±0.8	$< 10^{-8}$
HD 46375	21jan08	ESPaDOnS	486.83395	07:54:05	4×560	670	0.317	-0.900	0.46	3.0±0.6	$< 10^{-8}$
HD 46375	22jan08	ESPaDOnS	487.88189	09:03:10	4×560	670	0.342	-0.953	0.46	3.1±0.6	$< 10^{-8}$
HD 46375	23jan08	ESPaDOnS	488.91150	09:45:52	4×780	770	0.366	-0.992	0.39	2.5±0.5	$< 10^{-8}$
HD 46375	24jan08	ESPaDOnS	489.90655	09:38:48	4×780	780	0.390	-0.920	0.39	3.0±0.5	$< 10^{-8}$
HD 46375	25jan08	ESPaDOnS	490.87263	08:50:01	4×630	770	0.413	-0.911	0.40	2.5±0.5	$< 10^{-8}$
HD 46375	26jan08	ESPaDOnS	491.83784	07:59:59	4×630	650	0.436	-0.956	0.43	2.7±0.6	$< 10^{-8}$
HD 46375	27jan08	ESPaDOnS	492.79308	06:55:35	4×800	690	0.459	-0.889	0.40	2.4±0.5	$< 10^{-8}$
HD 130322	20jan08	ESPaDOnS	486.17067	16:07:04	4×560.0	670	-0.059	-12.244	0.44	1.0 ±1.1	$4.482 \times 10^{-4}$
HD 130322	21jan08	ESPaDOnS	487.17020	16:06:14	4×560.0	620	-0.020	-12.292	0.48	2.3 ±1.2	$1.580 \times 10^{-2}$
HD 130322	22jan08	ESPaDOnS	488.13040	15:08:47	4×780.0	730	0.017	-12.332	0.42	1.9 ±1.0	$1.219 \times 10^{-3}$
HD 130322	23jan08	ESPaDOnS	489.13228	15:11:22	4×700.0	700	0.055	-12.342	0.43	3.2 ±1.1	$1.229 \times 10^{-2}$
HD 130322	24jan08	ESPaDOnS	490.13394	15:13:37	4×700.0	650	0.094	-12.304	0.47	1.7 ±1.2	$1.129 \times 10^{-2}$
HD 130322	25jan08	ESPaDOnS	491.11998	14:53:22	2×630.0	410	0.131	-12.227	0.68	-0.8 ±1.7	$5.418 \times 10^{-1}$
HD 130322	27jan08	ESPaDOnS	493.13465	15:14:12	4×700.0	610	0.209	-12.124	0.46	2.7 ±1.1	$< 10^{-8}$
HD 130322	28jan08	ESPaDOnS	494.13485	15:14:21	4×700.0	540	0.247	-12.124	0.51	3.2 ±1.3	$9.045 \times 10^{-6}$
HD 130322	30jan08	ESPaDOnS	496.16789	16:01:39	2×650.0	370	0.326	-12.213	0.77	5.9 ±1.9	$2.070 \times 10^{-5}$

**Table A3.** Journal of observations of four stars for which the magnetic field is not detected.

Star	Date	Instrument	HJD (245 4000+)	UT time (h:m:s)	$T_{exp}$ (s)	S/N	$\phi_{rot}$	RV (km s <sup>-1</sup> )	$\sigma_{LSD}$ (10 <sup>-4</sup> $I_c$ )
XO-3	14oct09	ESPaDOnS	753.914090	09:50:38	4×860	310	0.8911	-12.663	0.90
XO-3	14oct09	ESPaDOnS	754.007340	12:04:54	4×860	250	0.9156	-12.706	1.14
XO-3	14oct09	ESPaDOnS	754.101130	14:19:58	4×(860)	310	0.9403	-12.730	0.87
XO-3	15oct09	ESPaDOnS	754.951580	10:44:35	4×860	290	1.1641	-11.998	0.93
XO-3	15oct09	ESPaDOnS	755.030280	12:37:55	4×860	310	1.1848	-11.840	0.87
XO-3	15oct09	ESPaDOnS	755.123800	14:52:35	4×860	240	1.2094	-11.590	1.14
XO-3	16oct09	ESPaDOnS	755.929600	10:12:55	4×860	130	1.4215	-10.170	2.27
XO-3	16oct09	ESPaDOnS	756.022450	12:26:37	4×860	100	1.4459	-10.398	3.38
XO-3	16oct09	ESPaDOnS	756.129000	15:00:03	4×860	50	1.4739	-10.237	9.12
XO-3	17oct09	ESPaDOnS	756.896140	09:24:42	4×860	160	1.6758	-12.451	1.88
XO-3	17oct09	ESPaDOnS	757.009760	12:08:19	4×860	90	1.7057	-12.285	3.81
XO-3	18oct09	ESPaDOnS	757.890810	09:17:01	4×860	310	1.9376	-12.478	0.89
XO-3	18oct09	ESPaDOnS	757.999710	11:53:49	4×860	290	1.9662	-12.338	0.92
XO-3	18oct09	ESPaDOnS	758.092700	14:07:44	4×860	300	1.9907	-12.175	0.91
XO-3	19oct09	ESPaDOnS	758.924770	10:05:53	4×860	300	2.2097	-9.862	0.92
XO-3	19oct09	ESPaDOnS	759.028770	12:35:39	4×860	300	2.2370	-10.000	0.89
XO-3	19oct09	ESPaDOnS	759.122950	14:51:16	4×860	290	2.2618	-10.271	0.95
XO-3	20oct09	ESPaDOnS	759.898910	09:28:38	4×860	290	2.4660	-12.298	0.94
XO-3	20oct09	ESPaDOnS	759.987590	11:36:20	4×860	290	2.4894	-12.440	0.93
XO-3	20oct09	ESPaDOnS	760.076200	13:43:56	4×860	290	2.5127	-12.540	0.94
HAT-P-2	26jun07	ESPaDOnS	277.780050	06:38:01	4×900	470	0.6472	-19.115	0.55
HAT-P-2	27jun07	ESPaDOnS	278.797830	07:03:38	4×800	500	0.9082	-19.254	0.51
HAT-P-2	28jun07	ESPaDOnS	279.793500	06:57:25	4×900	500	1.1635	-19.490	0.51
HAT-P-2	01jul07	ESPaDOnS	282.791670	06:54:50	4×900	500	1.9322	-19.164	0.53
Corot-7	05jan10	Narval	1202.515870	24:15:19	4×2000	120	52.9038	31.264	3.08
Corot-7	06jan10	Narval	1203.495410	23:45:52	4×2000	80	53.2805	31.226	4.87
Corot-7	18jan10	Narval	1215.489870	23:38:10	4×2000	90	57.8938	31.234	4.73
Corot-7	27jan10	Narval	1224.459390	22:54:42	4×2000	130	61.3436	31.188	2.87